Steric Crowding and the Kinetics of DNA Hybridization within a DNA Nanostructure System

Andre V. Pinheiro,[†] Jeanette Nangreave,[†,‡] Shuoxing Jiang,[†,‡] Hao Yan,[†,‡] and Yan Liu[†,‡,*]

[†]The Biodesign Institute and [‡]Department of Chemistry and Biochemistry, Arizona State University, Tempe, Arizona, United States

ABSTRACT

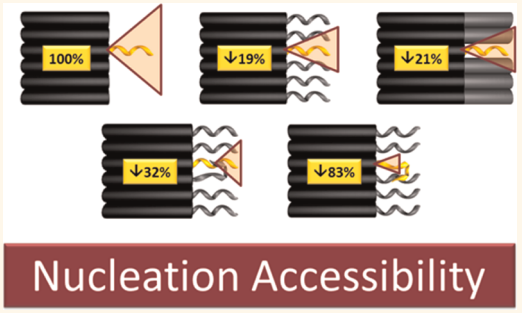

The ability to generate precisely designed molecular networks and modulate the surrounding environment is vital for fundamental studies of chemical reactions. DNA nanotechnology simultaneously affords versatility and modularity for the construction of tailored molecular environments. We systematically studied the effects of steric crowding on the hybridization of a 20 nucleotide (nt) single-stranded DNA (ssDNA) target to a complementary probe strand extended from a rectangular six-helix tile, where the number and character of the surrounding strands influence the molecular environment of the hybridization site. The hybridization events were monitored through an increase in the quantum yield of a single reporter fluorophore (5-carboxyfluorescein) upon hybridization of the 20-nt ssDNA, an effect previously undocumented in similar systems. We observed that as the hybridization site moved from outer to inner positions along the DNA tile, the hybridization rate constant decreased. A similar rate decrease was observed when noncomplementary single- and double-stranded DNA flanked the hybridization site. However, base-pairing interactions between the hybridization site of the probe and the surrounding DNA resulted in a reduction in the reaction kinetics. The decreases in the hybridization rate constants can be explained by the reduced probability of successful nucleation of the invading ssDNA target to the complementary probe.

KEYWORDS: DNA nanotechnology · hybridization kinetics · self-assembly · dynamic DNA nanostructures · single-stranded DNA probe

Understanding how the local molecular environment affects the kinetics of a chemical reaction is of great interest both to basic science and for technological applications. For example, the ultraefficient electron transfer present in photosynthetic systems is due to the precise arrangement of various protein and chromophore components, and the heterogeneous catalytic reactions widely used in the chemical industry are reliant on large surface areas with very specific microenvironments. However, among the tools and approaches we use to modulate molecular surroundings for the study of chemical reactions, few offer the spatial accuracy and versatility of structural DNA nanotechnology. In recent years, DNA nanostructures have become an attractive platform to organize matter at the molecular level, due to the reliability of base-pair interactions, improved DNA manipulation techniques, and affordable custom oligonucleotide synthesis. A variety of discrete, nanometer-sized structures with arbitrary shapes and designs are readily assembled with high yield.[1−4] The relative positions of molecules and the number and spacing of the surrounding molecular interactions are easily controlled using this method.

As new DNA nanostructure design strategies have evolved to support enhanced structural complexity and function, interest in dynamic structures has grown.[5,6] The latest dynamic DNA assemblies interact with the surrounding environment, respond to external stimuli with concomitant state changes, and even actuate according to programmed responses. Some examples include reconfigurable topological structures,[7] a wire-frame tetrahedron with controllable dimensions,[8] nanotubes for the controlled release of gold nanoparticles,[9] and DNA walkers.[10−12] Also, the development of DNA computing[13−16] enables researchers to embed the path to a desired end state within the DNA nanostructures themselves, with an external input triggering an automatic system response. Understanding how individual molecular components interact with one another is vital and may lead to improved design rules and active motifs for the construction of dynamic DNA structures.

* Address correspondence to yan_liu@asu.edu.

Received for review April 2, 2012 and accepted May 5, 2012.

Published online May 05, 2012
10.1021/nn301448y

© 2012 American Chemical Society

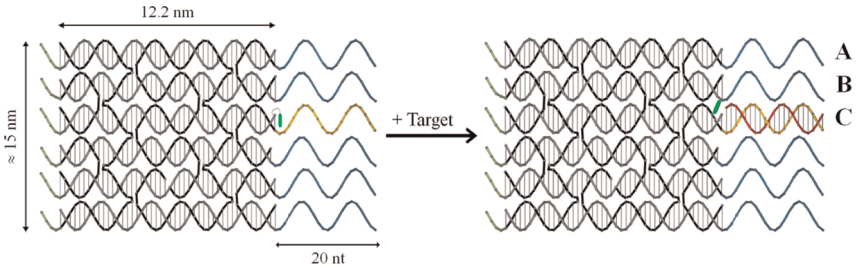

Figure 1. Detailed helical structure of one of the 6HX tiles used in this study. The core region of the tile is shown in gray and black. The schematic shown here corresponds to the design in which the target probe (yellow, 20-nt), extending from the right side of the core on the third helix from the top (position C), is surrounded by single-stranded off-target probes (blue, 20-nt) at every other position. Poly T sequences (T_{20}) for the off-target probes were used to minimize base-pairing interactions between the probes. The 5-carboxyfluorescein (FAM) reporter is covalently attached to the 5′ end of one of the DNA of the helices through a flexible linker (green), at the interface between the core and the target probe (position C). Poly T extensions (T_4), at every helical position on the left side of the core (dark green), prevent nonspecific dimerization of the tiles. The target (red) hybridizes to the target probe on helix three, forming a 20-bp duplex. If the target probe is extended from the end of helix 1 or helix 2, it is referred to as position A or position B, respectively. In those cases, the FAM reporter dye is attached to the end of the corresponding helix (not shown here).

The fate of a dynamic DNA structure is often governed by the kinetics of hybridization between interacting DNA strands[17−19] rather than the initial trigger. Therefore, many different strategies can be used to modulate the changes of state, including strand displacement, oligomerization of monomeric units, binding and release of protein−aptamer complexes, interaction with DNA binding proteins or small molecules (hormones, ATP, lipids, *etc.*), light-switchable cross-linking, secondary structure changes with varying pH, or interaction with other heteroelements (such as single-wall carbon nanotubes or metal nanoparticles). Understanding the factors that govern the hybridization kinetics and the ability to adjust them are extremely important for the design and functionality of these dynamic structures.

The thermodynamics and kinetics of nucleic acid hybridization have been thoroughly studied,[20−28] but few reports describe the behavior of complex structures that involve more than two or three DNA strands. The thermodynamics of DNA tile dimerization has been investigated by our group[29,30] and others;[24] however, no systematic study of the hybridization kinetics of DNA nanostructures has been reported. Here, we examined several steric factors that affect the kinetics of DNA hybridization within a DNA nanostructure. Our model system consists of a 20-nucleotide (nt) single-stranded DNA (ssDNA) target that is designed to hybridize to a complementary single-stranded probe extended from one of the helical ends of a rectangular six-helix DNA tile. The steric factors that were evaluated include (1) the position of the target probe relative to the tile; (2) the presence/absence of DNA surrounding the hybridization site; and (3) the formation of a double-helical secondary structure between the target probe and other components of the tile.

RESULTS AND DISCUSSION

System Model and Measurements. In our model, a 20-nucleotide DNA target strand hybridizes to a target probe (TP) displayed at specific positions along one side of a six-helix (6HX) DNA tile (Figure 1). The six-helix tile was adapted from previous reports[29,31] and consists of six parallel double helices joined by oligonucleotides that cross over from one helix to adjacent helices. This arrangement of helices results in a planar, rectangular-shaped tile (~16 nm long and 14 nm wide); the 14 constituent oligomers self-assemble into the desired tile when mixed together and annealed. The 3′ termini of selected helices were extended by 20 nucleotides, generating single-stranded overhangs that are designated as target probe or off-target probe (OTP) sequences. Target and off-target strands, each 20-nt long, are fully complementary to the target- and off-target probes, respectively. For all experiments, only one of the selected helices displayed the TP, while the remaining five helices were either blunt ends or displayed the OTP probes. This design permits accurate control of the number of strands surrounding the hybridization site, as well as the distance between the hybridization site and the neighboring strands.

To determine how binding site accessibility affected the rate of hybridization, several degrees of "crowding" of the TP were simulated. First, the effect of TP position was evaluated. The TP was displayed from each of the three different positions relative to the edge of the tile (Figure 1, outermost, position A; inner, position B; and innermost, position C, helices). The local environment of the TP at each position is unique, with accessibility decreasing as the TP moves inward (A > B > C). Second, the effect of single- and double-stranded DNA surrounding the hybridization site was evaluated (Figure 2). Three sets of experiments were performed: [1] The TP was surrounded by blunt-ended helices; that is, each of the five non-TP positions did not contain an OTP (Figure 2, left). This represents the least crowded scenario (Figure S1). [2] The TP was crowded by single-stranded DNA at the surrounding positions (Figure 2, center). Each of the five non-TP helices displayed a 20-nt poly(T) sequence to minimize

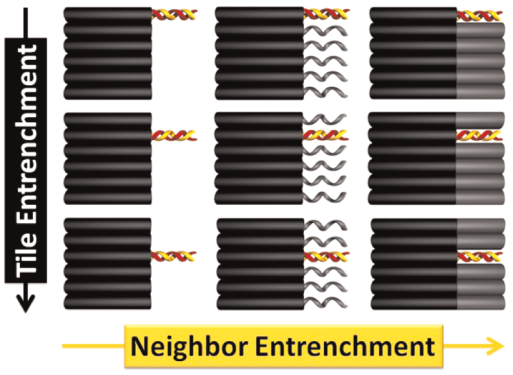

Figure 2. Schematic representation of the series of 6HX tiles used to determine the effect of steric accessibility of the binding site on the rate of hybridization. From top to bottom, the site of target hybridization is located at position A, B, and C, respectively. From left to right, the site of target hybridization is surrounded by blunt-end helices and crowded by single- and double-stranded DNA, respectively. Accessibility of the target to the target probe is expected to decrease from top to bottom and from left to right.

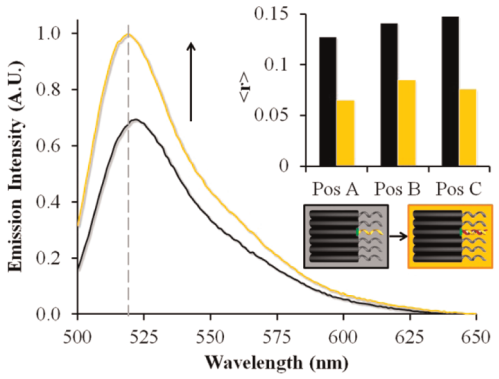

Figure 3. Fluorescence enhancement of the FAM reporter dye upon hybridization of the target to the 6HX tile. The fluorescence emission spectrum of FAM was measured before (black trace) and after (yellow trace) the addition of target to the 6HX tiles. The data shown here correspond to the design in which the target probe is located at position C and single-stranded off-target probes surround the target probe site. The spectra show a ~30% increase in the fluorescence quantum yield of the dye after hybridization of the target and a blue shift of the emission peak. The steady-state fluorescence anisotropy was independently measured for 6HX tiles with the target probe and the FAM reporter dye located at helical positions A–C. The inset summarizes the results of anisotropy measurements before (black bars) and after (yellow bars) the addition of target. Before target hybridization (black bars), high anisotropy values for all three designs (0.127–0.147) were observed, indicating the dye has significantly impaired rotation. After target hybridization (yellow bars), the anisotropy values drop considerably (0.065–0.076) for all designs, demonstrating that the dye is experiencing a less obstructed rotation.

the interaction between the OTPs and the TP and target (Figure S2). [3] The TP was crowded by double-stranded DNA at the surrounding positions (Figure 2, right). Each of the five non-TP helices displayed a random, 20-nt sequence (Figure S3). A fully complementary 20-nt off-target was hybridized to the OTPs, forming double-stranded extensions.

The effect of base-pairing interactions between the TP and adjacent OTPs on the rate of target hybridization was also evaluated. For these experiments, the TP was displayed from position C (the innermost), while a single OTP (with a sequence designed to be partially complementary to the TP) was displayed from the adjacent helix. The remaining four OTP positions were extended with 20-nt poly(T) sequences (Figures S4–S7).

For each TP position, a reporter fluorophore (5-carboxyfluorescein, FAM) was introduced at the interface between the core and the single-stranded TP (Figure 1). Initially the hybridization kinetics were monitored by measuring Förster resonance energy transfer (FRET) between the FAM (donor)-labeled tile and a TAMRA (acceptor)-labeled target. However, even in the absence of the other dye, considerable changes in the fluorescence quantum yields of both dyes were observed upon hybridization. For FAM-labeled tiles, a 15–40% increase in fluorescence quantum yield was detected upon hybridization of an unlabeled target (Figure 3 and Figures S11 and 12), and for TAMRA-labeled target, ~30% quenching was observed upon its hybridization to an unlabeled tile (Figure S8). These changes in quantum yield are opposite the characteristic decrease in donor emission and increase in acceptor emission that are expected to occur in FRET, which would significantly complicate analysis of the efficiency of energy transfer and render this method unsuitable for monitoring the hybridization events. However, the increase in quantum yield of FAM after hybridization was evaluated further, as shown in Figure 3. We determined that FAM alone could be used to monitor hybridization.

First, the increase in quantum yield and slight blue shift (2–4 nm) clearly indicate that hybridization induces a change in the molecular environment of the fluorophore (Figure 3). Time-correlated fluorescence single photon counting (TC-SPC) was used to measure the fluorophore decay times. In the absence of the target, the fluorescence decay was well fit by a biexponential law with two time constants: 4.4 ns (92%) and 1.7 ns (8%) (Figure S9). The 4.4 ns decay corresponds to the lifetime of free FAM dye in aqueous solution.[32] After equilibrating with an excess of target, the fluorescence decay was dominated by the slower component (4.1 ns, 98%), with the amplitude of the faster component (1.7 ns) only ~2% (Figure S9). The results show that hybridization of the target to the 6HX tile promotes the conversion of a short-lived FAM excited state to a longer-lived excited state. No change in the extinction coefficients of absorption "before" and "after" target addition was observed. Therefore, the increase in fluorescence quantum yield and decrease of the short lifetime component after hybridization can be explained by a decrease in the nonradiative decay rate constant of the dye. This indicates that after hybridization the dye is subject to a local environment with fewer quenching factors.

Next, steady-state fluorescence anisotropy measurements were performed (each of the three FAM-labeled probe positions were independently evaluated), before and after target hybridization (inset Figure 3). Before hybridization, high anisotropy values (0.127–0.147) were observed, which are slightly higher than the anisotropy values for linear DNA strands terminally functionalized with fluorescein.[33,34] This demonstrates that the FAM dye attached to the end of the DNA tile (Figure 1, left) experiences restricted rotation during excited-state deactivation. After the addition of target, the anisotropy decreased considerably to 0.065–0.076, signifying that the hybridization event leads to increased free rotation of the dye. Taken together, the TC-SPC and anisotropy results suggest that before hybridization a fraction of the FAM population may be intercalated within the single-stranded TP or stacked with the adjacent base at the end of the corresponding DNA helix (Figure 1, left), where the rotational dynamics of the dye is expected to be highly restricted. Stacking with adjacent bases leads to a lower quantum yield and faster decay, probably the result of photoinduced electron transfer from FAM to the adenine bases flanking the dye, as was observed in simpler systems.[32,35] The conformational rigidity of the DNA nanostructure is likely to enhance the effect of photoinduced electron transfer, more commonly observed when guanine bases are in the vicinity of the FAM dye.[36,37] Upon target hybridization, the formation of a double helix displaces the dye from its intercalated or stacked state, reducing the interaction of the dye with the TP or the core tile structure (Figure 1, right). This would explain the drastically decreased anisotropy, increased emission, and increased amplitude of the longer lifetime component of the fluorescence decay.

Finally, we verified that the increase in quantum yield is site specific, occurring only when the target hybridizes to the FAM-labeled position of the tile. We designed a series of 6HX tiles in which the TP was systematically displayed from each helical position, while the FAM reporter was held constant at position C. The steady-state fluorescence emission of each tile was independently measured before and after the addition of target (Figure S10). The enhancement in fluorescence was observed only when the TP was displayed from position C (Figure 4). Similar results were obtained for tiles with FAM labels at positions A and B (Figures S11 and S12). The results suggest that the displacement of the dye from an intercalated or stacked state involves a change in the specific local environment. The single-dye approach presented here offers an advantage over the FRET approach, because it allows the addition of a large excess of unlabeled target strand, simplifying the reaction rate determination.

To determine the extent of the forward and reverse hybridization reaction, gel electrophoretic analysis and steady-state fluorescence analysis of the equilibrium

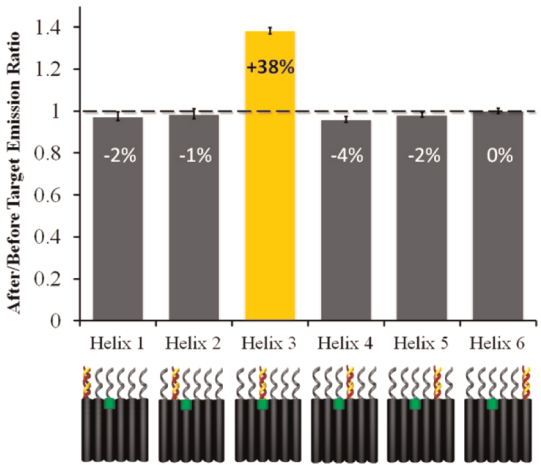

Figure 4. Site specificity of the FAM single-dye reporter system. The steady-state fluorescence emission of six designs was independently evaluated, where the helical position of the target probe was systematically displayed from each helix, while the position of the FAM dye remained constant on helix 3. Each design corresponds to a situation in which the site of the target probe is surrounded by single-stranded off-target probes. The bar graph shows the ratio of emission intensity after and before the addition of the target. The emission of the FAM dye exhibited ~40% enhancement (yellow bar) only when the target probe was located on helix 3.

products were performed. The gel shift assays show that with a 5-fold excess of the target all the 6HX tile is consumed (within detection limits) to produce a tile/target hybridized product (Figures S13–S17). In addition, the steady-state fluorescent intensity of several FAM-labeled 6HX tile solutions was measured at 1:1, 2:1, and 10:1 target:tile ratios. The maximum intensity of emission did not increase when the ratio of target:tile exceeded 1:1 (Figure S18), verifying the stoichiometric completion of the forward hybridization reaction.

Dependence of the Hybridization Rate on Accessibility of the Binding Site. For the simplest system, in which the target hybridizes to a single TP in the absence of OTPs, hybridization is expected to follow a two-step mechanism: nucleation of a short segment of the incoming target to the TP, followed by realignment of both strands and "zipping" of the remaining nucleotides for fully complementary base-pairing.[21] Nucleation is the rate-limiting step of hybridization at low DNA concentrations (nano- to micromolar range), relying on efficient collisions between the interacting strands. The subsequent strand realignment and fully complementary base-pairing are expected to proceed at a much faster rate. In our system, the fluorescence enhancement of the reporter dye occurs only after the 3′ terminal nucleotides of the target form base pairs with the 5′ termini of the TP (adjacent to the core where the dye is located). Consequently, hybridization of the target to the TP can be simplified to a bimolecular process with an overall rate constant of k_{hyb}. A large excess of target strand further simplifies the kinetics and facilitates application of a pseudo-first-order

kinetic model. To verify pseudo-first-order behavior, the reaction was carried out at several different 6HX tile concentrations, with a constant target concentration (minimum 10-fold excess) The linear dependence of the rate constant as a function of the tile concentration, as shown in Figure S19, confirms that a pseudo-first-order kinetic model is valid. This method simplifies the data analysis, allowing a single-exponential kinetic model to be used to fit the kinetic data, increasing the accuracy of the calculated rate constant.

Figure 5 shows the change in fluorescence intensity of the FAM reporter as a function of time after the addition of a 20-fold excess of target to a 6HX tile solution (1 nM). The 6HX tiles had a TP displayed at position C and no DNA surrounding the site of hybridization. The resulting curve was well fit by a monoexponential growth equation, yielding a bimolecular rate constant of $(1.04 \pm 0.05) \times 10^6\ s^{-1}\ M^{-1}$. This value is consistent with the bimolecular rate constants obtained from other studies of simple nucleic acid association kinetics.[38] 6HX tiles with TPs displayed at positions A and B (with the corresponding FAM reporters at positions A and B, respectively) were also examined. An ~10% decrease in the hybridization rate constants were observed for the interior positions (Figure 6, left series). The decrease in the rate of hybridization can be attributed to the reduced accessibility of the TP at the inner positions (B and C).

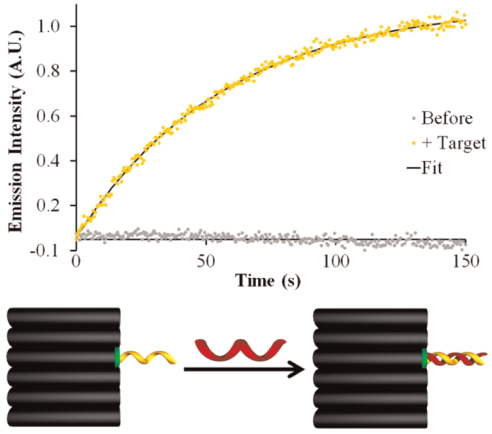

Figure 5. Monitoring the hybridization of a 20-nt DNA target to a complementary target probe displayed from a 6HX Tile. The data shown here correspond to a design in which the target probe is located at position C, without neighboring off-target probes. The hybridization event is monitored in real time by measuring the emission intensity of FAM as the local environment of the dye changes. Before the addition of target (schematic, left), the fluorescence emission of a 1 nM 6HX tile solution was measured for 150 s, providing a baseline signal (gray series). Immediately after the addition of 20 equivalents of target, the fluorescence intensity of the same solution was monitored in real time (yellow series). The resulting curve was fit by a monoexponential growth equation, from which the bimolecular rate constant of the overall hybridization reaction was calculated.

When single-stranded OTPs were displayed from the other five helices flanking the TP, a further decrease in the hybridization rate constant was observed (for all three positions; Figure 6, middle panel). The single-stranded DNA surrounding the hybridization site is likely to impair the approach of the target strand and, consequently, reduce the rate of efficient collisions necessary for nucleation. It is interesting that single-stranded DNA surrounding the hybridization site results in a noticeable difference between the hybridization rates at positions B and C (Figure 6, middle panel), an effect that is not as significant for 6HX tiles with no OTPs (Figure 6, left panel). This result confirms that the DNA strands flanking the hybridization site further reduce the accessibility of the TP.

6HX tiles with double-stranded DNA surrounding the TP were also evaluated (Figure 6, right panel). We expected that double-stranded DNA would further reduce the steric accessibility of the TP, leading to a decrease in the overall rate of hybridization. However, the results revealed no significant changes in the rate constants, compared to all cases with single-stranded DNA flanking the TP. It is possible that the rigidity of

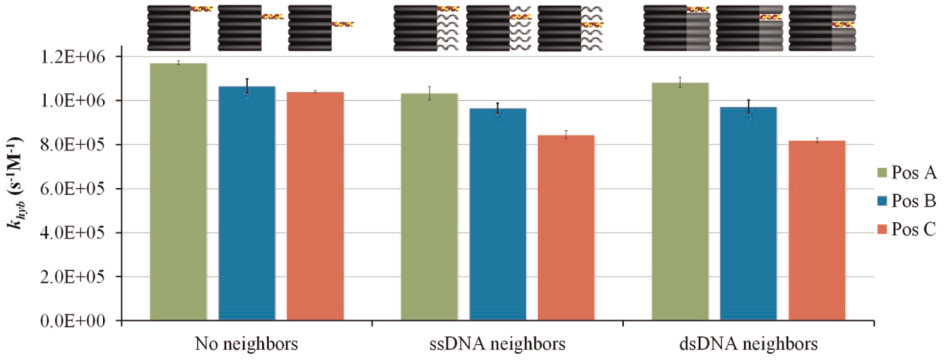

Figure 6. Summary of the observed hybridization rate constants for various levels of target binding site accessibility. The left three bars correspond to designs in which the target probe is not surrounded by single- or double-stranded DNA. The middle three bars correspond to designs in which the target probe is crowded by single-stranded off-target probes. The three bars on the right correspond to designs in which the target probe is crowded by double-stranded DNA. For all three sets of data, the green, blue, and red bars represent the measured rate constants for the designs in which the target probe is located at positions A, B, and C, respectively. The error bars are the standard deviation of 5–8 replicate measurements.

TABLE 1. Activation Energies for the Hybridization of a Single-Stranded DNA Target to a 6HX Tile for Each of the Designs Shown in Figure 6[a]

	target probe position	activation energy (kcal mol^{-1})
no neighbors	position A	19.9 ± 0.1
	position B	18.6 ± 0.5
	position C	19.3 ± 0.3
ssDNA Neighbors	position A	20.4 ± 0.6
	position B	19.9 ± 0.4
	position C	20.0 ± 0.5
dsDNA Neighbors	position A	18.4 ± 0.1
	position B	19.4 ± 0.8
	position C	20.1 ± 0.4

[a] Regardless of the target probe position, or the presence/absence of DNA surrounding the target probe, the activation energy required to initiate target hybridization is approximately 18−20 kcal/mol. The errors correspond to the uncertainty in the slope of the linear fit of the Arrhenius plot (Figures S20−S22).

double-stranded DNA restricts the range of available spatial orientations of the OTPs, and this will counteract the effects of increased mass (crowding) and result in kinetics that are similar to the single-stranded case. The decrease in the rate of hybridization is similar to what was observed when the position of the TP was moved from position A to C.

Researchers have speculated that there are positional and steric factors that influence the equilibrium and kinetics of hybridization of a DNA nanostructure probe to an external target strand.[39,40] The group of experiments reported here represents the first attempt to obtain quantitative information about these effects. The observed rate constants are 4 orders of magnitude slower than diffusion-limited bimolecular reaction kinetics, indicating a high activation energy barrier for the rate-limiting step. We propose that variations in the rate constants are a direct consequence of the spatial crowding of the TP in the DNA tile by the presence of other DNA structures.

To clarify whether the nucleation step, realignment of the nucleated target, or both were affected by steric crowding, temperature-dependent hybridization kinetics were measured for all the previously mentioned designs. Arrhenius plots were used to obtain the activation energies of the reactions (Figures S20−22). Typical Arrhenius behavior was observed in all cases (Figures S20−S22), and linear fits of the plots yielded positive activation energies (Table 1). The magnitudes of the activation energies were in a narrow range (∼18−20 kcal/mol) for all designs. The activation energies of the hybridization reactions described here include the free energies required to rotate and realign the target/TP pairs and to overcome the charge repulsion and solvent reorganization to induce a conformational change from a random coil (ssDNA) to a helical structure (dsDNA). The influence of electrostatic repulsion between negatively charged DNA tiles and the DNA target is assumed to be negligible due to the high concentration of magnesium in solution (12.5 mM), compared to the concentration of DNA tiles (1 nM).

The fairly large activation energies that were obtained support our conclusion that the rates of the hybridization reactions are not simply diffusion limited. However, due to the relatively large errors in the activation energy measurements (even a small difference in the activation energy, *e.g.*, ∼0.1 kcal/mol, can cause a measurable change in the reaction rate), it is not a straightforward task to conclude exactly how steric crowding affects each step of hybridization. It is reasonable to suggest that the observed differences in kinetics are mainly due to differences in the frequency of effective collisions that lead to complete hybridization between the two strands. Thus, in a more spatially confined environment, less effective nucleation is responsible for slower hybridization kinetics.

Effects of Target Probe−Off Target Probe Interactions. In addition to evaluating the steric crowding effect on the rate of hybridization, we also characterized how the interaction of the TP with other components of the tile influenced the rate of hybridization. From a practical standpoint, there are many situations in which a given "probe" sequence is flanked by neighboring single-stranded DNA of a different sequence. As the length of the strands increases, there is greater probability of partial sequence complementarily between the strands. When there are base-pairing interactions between the TP and adjacent single-stranded DNA, complete hybridization of the target can be achieved only through an additional strand displacement reaction.[41] In this case, hybridization of the target to the 6HX tile can no longer be regarded as a straightforward bimolecular event, but rather a more complex process involving at least three-steps: (1) nucleation of the incoming target with a single-stranded segment of the TP, (2) realignment and partial hybridization of the strands, and (3) displacement of the neighboring, partially hybridized single-stranded DNA from the TP, until full hybridization of the target strand is achieved. It should be noted that the interaction of the TP with adjacent, single-stranded DNA in a DNA tile is an intramolecular interaction. As a consequence, the "local molecular concentration" increases dramatically and the frequency of collisions that may lead to a TP−ssNeighbor complex is greater than for free strands in solution.

In our design, the TP and OTPs are arranged parallel to one another, with the same polarity. In order to create partial complementarity between the probes, one of the strands must reverse direction so that antiparallel base-pairing can occur. Two different configurations of TP-OTP interactions were considered: (1) the OTP reverses direction and binds to the TP, and (2) the TP reverses direction and binds to an adjacent OTP (Figure 7). For all corresponding designs, the TP and

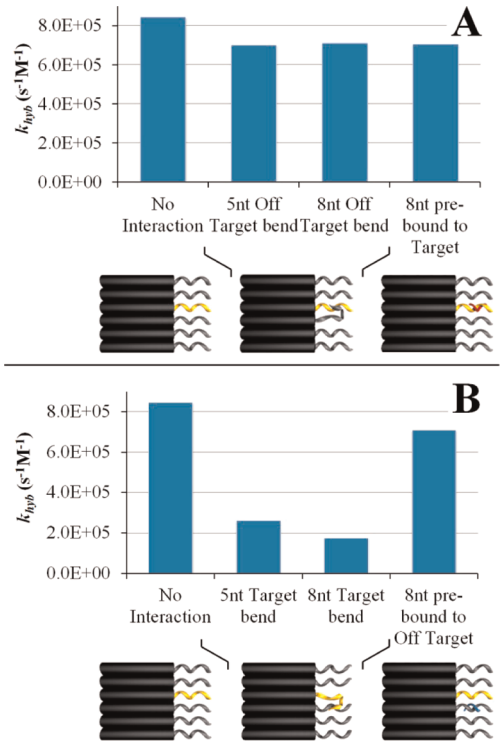

Figure 7. Summary of observed hybridization rate constants for designs with various probe interactions. The target probe is located at position C for all cases. The sequences of the off-target probes were modified to introduce specific base-paring interactions between the target and off-target probes. (A) When the 3′ end of the off-target probe has a sequence designed to be complementary to the middle section of the target probe, it bends toward the target probe, forming a 5- or 8-bp double helix (two middle bars). Both modifications result in a similar reduction (~17%) in the hybridization rate constant compared to the original design without any complementarity between the target and off-target probes (left bar). Experiments with a prebound, 8-nt truncated target that must be displaced by the full length target (right bar) result in similar kinetics. (B) When the 3′ end of the target probe is designed to be complementary to the middle section of the off-target probe, the 3′ end of the target probe bends toward the off-target probe, forming a 5- or 8-bp double helix (two middle bars). Both modifications result in significant reduction of the hybridization rate constant, 70% and 79%, respectively, compared to experiments with no interactions between the probes (left bar). The bar on the right reveals that the rate constant is restored by prebinding an 8-nt truncated target to the target probe binding domain of the off-target probe.

the FAM reporter dye were located at helical position C. The kinetics of hybridization was measured as described previously, and the resulting fluorescence signals were fit by a monoexponential growth law. The observed rate constants represent a combination of all three hybridization steps: nucleation, realignment, and strand displacement.

First we evaluated the situation in which an OTP reverses direction to partially hybridize with the TP (Figure S4). An 8-nt domain complementary to the TP was inserted into the OTP so that the OTP would hybridize with the middle section of the TP, leaving an 8-nt toehold at the 3′ end of the TP to serve as a docking station for the incoming target. Compared to the case of a 6HX tile with no base-pair interactions between the probes, a 17% decrease in the hybridization rate constant was observed (Figure 7A). When the sequence of the OTP was modified to allow the formation of only 5 base-pairs (rather than 8) with the TP (Figure S5), no change in the rate was observed. We performed a control experiment with an 8-nt truncated target (TT) that was prehybridized to the same 8-nt domain of the TP, and a similar rate constant was observed. It should be noted that the 8-nt docking domain at the 3′ end of the TP was the same for all three cases. This group of experiments shows that the presence of secondary structure (bending) in the OTP does not affect the rate of hybridization, and the 17% decrease in the hybridization rate reflects only the displacement of the 8-nt domain of the OTP or the TT. The frequency of effective collisions at the nucleation site is expected to be lower due to the reduced number of nucleotides accessible for nucleation.

Zhang and Winfree[42] demonstrated a model in which the kinetics of strand displacement reactions is dependent on the toehold length (and toehold AT/GC content). The authors relate an increase in the rate constant with higher toehold binding energy. Their model predicts that an 8-nt long toehold will have a rate constant between 10^5 and 10^6 M^{-1} s^{-1}, depending on the AT/GC content. This result is on the same order of magnitude as the hybridization rate constants measured in our system. It should be noted that in their study Zhang and Winfree[42] used simple DNA oligonucleotides, where the sequences were designed to eliminate any undesirable secondary structure. In our study, secondary structure was intentionally introduced and one of the participants was a 6HX tile with much slower diffusion than simple single-stranded DNA, so it is difficult to quantitatively compare the two results. However, some qualitative information can still be inferred. Zhang and Winfree[42] proposed a reasonable simplification of their three-step kinetic model (for toehold lengths greater than 5-nt), where the overall rate constant of a strand displacement reaction is approximately equal to the rate constant of the nucleation/zipping phase of hybridization. This corresponds to the set of experiments described here, in which an 8-nt toehold was used. Therefore, it is reasonable to assume that the observed decrease in the rate constant of target hybridization is due to a decrease in the number of nucleotides available for nucleation, rather than the presence of an additional strand displacement step.

Next, situation 2 was evaluated, where the 3′ end of the TP changes direction to interact with the OTP. A rate constant of 3.1×10^5 M^{-1} s^{-1} was observed for a 5-bp interaction between the probes (Figure 7B), representing a ~70% decrease in the hybridization rate.

In this design, the 3′ end of the TP is blocked and not available for nucleation of the invading target. In order for the target to hybridize with the TP, it must first nucleate at the 5′ end of the TP, which is adjacent to the tile core and not as accessible as the 3′ end, and subsequently zip up and displace the OTP. When a longer, 8-bp interaction between the TP and OTP (Figure S7) was introduced, an additional decrease in the rate of target hybridization was observed (a 79% decrease compared to experiments with no interaction between probes, Figure 7B). Reduced accessibility and a further decrease in the number of nucleation sites are expected to contribute to the greatly reduced hybridization rate. Finally, as expected, when a free 8-nt strand was prehybridized to the interaction domain of the OTP to prevent the interprobe interaction, the hybridization rate increased to the expected level (Figure 7B).

We propose that all the changes in the hybridization rate constants reported here are governed by a single factor, the probability of effective nucleation. The rate of hybridization is determined by the frequency of successful collisions between the target and TP, which depends on the translational and rotational motion of the target. The studies reveal the importance of the following factors on the rate of hybridization: (1) the position of the TP within the tile and the presence of other DNA surrounding the site of hybridization, both of which restrict the range of effective encounter angles, (2) the length of the toehold that determines the initial nucleation binding energy, and (3) the distance of the nucleation site from the core of the tile and thus the accessibility of the site.

CONCLUSIONS

The results presented here strongly suggest that the rate constant of hybridization of a DNA strand to its complementary probe within a DNA tile is strongly dominated by a rate-limiting nucleation step. When DNA surrounds the hybridization site, the frequency of successful collisions and subsequently the hybridization rate of the target to the TP are reduced due to steric impairment of the target binding site. The hybridization rate is more severely affected when the only available site for target nucleation is adjacent to the tile core. The sequences of the target and the TP were held constant for all the experiments presented here, but it is reasonable to assume that changes in the sequences of the hybridization pairs may produce different behavior. Future experiments will address the effect of sequence and target length. These studies are necessary to develop a more comprehensive understanding of the hybridization kinetics in DNA nanostructures.

In DNA nanotechnology, it is crucial to understand how the thermodynamics and kinetics of the final structure formation are affected by the number, length, sequence, and structure of the strands connecting the supramolecular arrangements. We believe that the results presented here will contribute to a better understanding of the physical behavior of DNA nanostructures. It will be interesting to determine if the effects observed for a 1D arrangement of DNA probes will translate to more complex architectures and whether the effects will be amplified when multiple hybridization sites are present. The design of DNA walkers and other DNA-based motors will also benefit from such knowledge, where the arrangement of single-stranded extensions (or tracks) in 1D or 2D arrangements may be optimized by considering the effects of the surrounding local environment. The result suggests that the presence of double-stranded DNA will not affect the hybridization of the walker to a DNA tile any more than their single-stranded DNA counterparts. In addition, hybridization of DNA targets to a network of probes will likely occur at a faster rate for peripheral probes than for interior ones, and in the context of DNA-walkers, this may result in walker path bias. Finally, the application of microarray-based platforms for disease detection can benefit from improved sequence design and spatial control of the probes to enhance the kinetics of DNA hybridization.

MATERIAL AND METHODS

Self-Assembly of DNA Nanostructures. All DNA strands (Figures S1−S7) used for assembly of nanostructures were purchased from Integrated DNA Technologies, Inc. (www.idtdna.com) and purified by denaturing polyacrylamide gel electrophoresis (PAGE; 6−10% acrylamide in 1× TBE buffer: 89 mM Tris base, 89 mM boric acid, 2 mM EDTA, pH 8.0) for the unmodified DNA oligomers, or by HPLC for the dye-labeled DNA oligomers. The design of each 6HX tile included one oligomer modified with a FAM dye. The 6HX tiles were assembled by mixing equimolar amounts of all the oligomers present in the structures at a final concentration of 500 nM, in 1× TAE Mg^{2+} buffer (40 mM Tris base, 20 mM acetic acid, 2 mM EDTA·Na_2·$12H_2O$, 12.5 mM ($(CH_3COO)_2Mg·4H_2O$)), then by heating the mixtures at 90 °C and cooling to 4 °C over 12 h using an automated PCR thermocycler (Mastercycler Pro, Eppendorf).

Fluorescence Measurements. All the fluorescence decay measurements were collected using a time-correlated single-photon-counting method using a titanium sapphire laser (Millennia/Tsunami, Spectra Physics) with a 130 fs pulse duration operated at 80 MHz, in a 1 cm path length quartz cell (Hellma). The laser output was tuned to 740 nm and sent through a frequency doubler and pulse selector (Spectra Physics, model 3980) to obtain 370 nm excitations at 4 MHz. Fluorescence emission was collected at a right angle to the excitation beam and detected using a double-grating monochromator (Jobin-Yvon, Gemini-180) and a microchannel plate photomultiplier tube (Hamamatsu R3809U-50). Data acquisition was performed using a single photon counting card (Becker-Hickl, SPC-830), and the emission was collected at 520 nm. The instrument response function had a full width at half-maximum of 35−45 ps, as verified by scattering from samples. Global analysis was performed using the in-house software package ASUFIT. The lifetime of the fluorescence decay of FAM in the 6HX tiles, before and after target hybridization, was obtained using the system described above; unless otherwise indicated, 120 μL of 250 nM 6HX tile solution was used for these measurements.

All steady-state and real-time fluorescence spectra were measured by a Nanolog fluorometer (Horiba Jobin Yvon, L-format, equipped with a CW 450 W xenon light source, thermoelectrically cooled R928 PMT, and fully automated excitation and emission polarizers for anisotropy measurements), with a 1 cm path length quartz cell (Hellma); all spectra were corrected for the wavelength dependence of the detection system response. For real-time analysis, the temperature of the quartz cell was controlled/held constant by a refrigerated water circulator (Thermoscientific). Unless otherwise indicated, 120 μL of 50 nM 6HX tile solution was used for measurements. Fluorescence emission spectra were collected using 475 nm excitation wavelength, 5 nm excitation slits, 485−650 nm emission wavelength range, 5 nm emission slits, and 1 s integration time. Fluorescence anisotropy was also measured in the same manner with 495 nm excitation wavelength, 5 nm excitation slits, 540 nm emission wavelength, 5 nm emission slits, and 10 s integration time. Anisotropy values were calculated from the instrument software FluorEssence for Windows by Horiba Scientific.

Real-Time Fluorescence Measurements. The kinetics of hybridization of a DNA target to a 6HX tile was monitored in real time via changes in a fluorescence dye reporter molecule, FAM, upon hybridization of the target. Unless otherwise indicated, 120 μL of 1 nM 6HX tile solution was used for measurements. The parameters used to collect real-time spectra were as follows: 485 nm excitation wavelength, 3 nm excitation slits, 520 nm emission wavelength, 15 nm emission slits, and 0.5 or 1 s integration time depending on the total measurement time. The temperature of the sample was held constant for all real-time data collection. The following temperatures were used to generate Arrhenius plots: 11, 14, 16, 18, and 20 °C.

First, the temperature of the fluorometer cell holder and the 6HX tile sample under investigation was allowed to equilibrate for 5 to 7 min. Then, the fluorescent signal of the 6HX tile solution was collected for 150−350 s (depending on the experiment) to confirm the photostability of the fluorophore with continuous exposure to the excitation source. A 2−5% reduction in the overall emission of the equilibrated solutions was observed for a typical measurement period. Next, data collection was initiated and 20 equivalents of unlabeled target was directly added to the cuvette secured in the instrument (in the dark). The solution was mixed by pipetting for 1−2 s, and the kinetics of hybridization of the target was followed by monitoring the intensity of FAM emission for the length of the reaction.

The kinetic measurements were repeated at least five times for every design under investigation. Several control experiments were performed to confirm that the target addition process resulted in homogeneous mixing and that the delay caused by the mixing was negligible compared to the hybridization kinetics. The kinetic curves were subsequently fit by a monoexponential growth model, and the bimolecular rate constants were extracted by dividing the time constant by the target concentration using OriginPro 8 (Origin Lab) software.

Native Gel Electrophoretic Characterization of Nanostructures. The correct assembly of all 6HX tile designs and subsequent hybridization of all target and off-target DNA were confirmed by nondenaturing polyacrylamide gel electrophoresis (Figures S8−S12). Structures (7 pmol of each 6HX tile, before and after addition of 5 equivalents of target) were analyzed by 5% nondenaturing PAGE gels in 1× TAE Mg buffer. Electrophoresis was performed at 200 V, 10−20 °C, for ∼4 h. The resulting gels were analyzed by a Typhoon Trio variable mode imager (GE Healthcare, excitation at 488 nm, emission at 520 nm) for visualization. The gels were subsequently stained with ethidium bromide and scanned in a Biorad Gel Doc XR+ system.

Conflict of Interest: The authors declare no competing financial interest.

Acknowledgment. This work was supported by grants from the Army Research Office, Office of Naval Research, National Science Foundation, Department of Energy, and National Institutes of Health to Y.L. Y.L. is also supported by the Technology and Research Initiative Fund from Arizona State University.

Supporting Information Available: Detailed information regarding structure design, electrophoretic analysis, and fluorescence characterization. This material is available free of charge via the Internet at http://pubs.acs.org.

REFERENCES AND NOTES

1. Aldaye, F. A.; Palmer, A. L.; Sleiman, H. F. Assembling Materials with DNA as the Guide. *Science* **2008**, *321*, 1795–1799.
2. Shih, W. M.; Lin, C. Knitting Complex Weaves with DNA Origami. *Curr. Opin. Struct. Biol.* **2010**, *20*, 276–282.
3. Kuzuya, A.; Komiyama, M. DNA Origami: Fold, Stick and Beyond. *Nanoscale* **2010**, *2*, 310–322.
4. Tørring, T.; Voigt, N. V.; Nangreave, J.; Yan, H.; Gothelf, K. V. DNA Origami: A Quantum Leap for Self-assembly of Complex Structures. *Chem. Soc. Rev.* **2011**, *40*, 5636–5646.
5. Pinheiro, A. V.; Han, D.; Shih, W. M.; Yan, H. Challenges and Opportunities for Structural DNA Nanotechnology. *Nat. Nanotechnol.* **2011**, *6*, 763–772.
6. Zhang, D. Y.; Seelig, G. Dynamic DNA Nanotechnology Using Strand-Displacement Reactions. *Nat. Chem.* **2011**, *3*, 103–113.
7. Han, D.; Pal, S.; Liu, Y.; Yan, H. Folding and Cutting DNA into Reconfigurable Topological Structures. *Nat. Nanotechnol.* **2010**, *5*, 712–717.
8. Goodman, R. P.; Heilemann, M.; Doose, S.; Erben, C. M.; Kapandis, A. N.; Turberfield, A. J. Reconfigurable, Braced, Three Dimensional DNA Nanostructures. *Nature* **2008**, *3*, 93–96.
9. Lo, P.; Karam, P.; Aldaye, F.; Hamblin, G.; Cosa, G.; Sleiman, H. Loading and Selective Release of Cargo in DNA Nanotubes with Longitudinal Variation. *Nat. Chem.* **2010**, *2*, 319–328.
10. Gu, H.; Chao, J.; Xiao, S. J.; Seeman, N. C. A Proximity-Based Programmable DNA Nanoscale Assembly Line. *Nature* **2010**, *465*, 202–205.
11. Lund, K.; Manzo, A. J.; Dabby, N.; Michelotti, N.; Johnson-Buck, A.; Nangreave, J.; Taylor, S.; Pei, R.; Stojanovic, M. N.; Walter, N. G.; et al. Molecular Robots Guided by Prescriptive Landscapes. *Nature* **2010**, *465*, 206–210.
12. Wickham, S. F. J.; Endo, M.; Katsuda, Y.; Hidaka, K.; Bath, J.; Sugiyama, H.; Turberfield, A. J. Direct Observation of Stepwise Movement of a Synthetic Molecular Transporter. *Nat. Nanotechnol.* **2011**, *6*, 166–169.
13. Chen, X.; Ellington, A. D. Shaping Up Nucleic Acid Computation. *Curr. Opin. Biotechnol.* **2010**, *21*, 392–400.
14. Stojanovic, M. N. Some Experiments and Directions in Molecular Computing and Robotics. *Isr. J. Chem.* **2011**, *51*, 99–105.
15. Yin, P.; Choi, H. M. T.; Calvert, C. R.; Pierce, N. A. Programming Bimolecular Self-assembly Pathways. *Nature* **2008**, *451*, 318–322.
16. Qian, L.; Winfree, E. Scaling Up Digital Circuit Computation with DNA Strand Displacement Cascades. *Science* **2011**, *332*, 1196–1201.
17. Dirks, R. M.; Pierce, N. A. P. Triggered Amplification by Hybridization Chain Reaction. *Proc. Natl. Acad. Sci. U. S. A.* **2004**, *101*, 15275–15278.
18. Choi, H. M. T.; Chang, J. Y.; Trinh, L. A.; Padilla, J. E.; Fraser, S. E.; Pierce, N. A. Programmable in Situ Amplification for Multiplexed Imaging of mRNA Expression. *Nat. Biotechnol.* **2010**, *28*, 1208–1212.
19. Delebecque, C. J.; Lindner, A. B.; Silver, P. A.; Aldaye, F. A. Organization of Intracellular Reactions with Rationally Designed RNA Assemblies. *Science* **2011**, *22*, 470–474.
20. Chen, C.; Wang, W.; Wang, Z; Wei, F.; Zhao, X. S. Influence of Secondary Structure on Kinetics and Reaction Mechanism of DNA Hybridization. *Nucleic Acids Res.* **2007**, *35*, 2875–2884.
21. Wetmur, J. G. Hybridization and Renaturation Kinetics of Nucleic Acids. *Annu. Rev. Biophys. Bioeng.* **1976**, *5*, 337–361.
22. Morrison, L. E.; Stols, L. M. Sensitive Fluorescence-Based Thermodynamic and Kinetic Measurements of DNA Hybridization in Solution. *Biochemistry* **1993**, *32*, 3095–3104.

23. Yin, Y.; Zhao, X. S. Kinetics and Dynamics of DNA Hybridization. *Acc. Chem. Res.* **2011**, *44*, 1172–1181.
24. Sacca, B.; Meyer, R.; Feldkamp, U.; Schroeder, H.; Niemeyer, C. M. High-throughput, Real-Time Monitoring of the Self-assembly of DNA Nanostructures by FRET Spectroscopy. *Angew. Chem., Int. Ed.* **2008**, *47*, 2135–2137.
25. Miyoshi, D.; Sugimoto, N. Molecular Crowding Effects on Structure and Stability of DNA. *Biochimie* **2008**, *90*, 1040–1051.
26. SantaLucia, J.; Hicks, D. The Thermodynamics of DNA Structural Motifs. *Annu. Rev. Biophys. Biomol. Struct.* **2004**, *33*, 415–440.
27. Yuan, B.; Zhuang, X.; Hao, Y.; Tan, Z. Kinetics of Base Stacking-Aided DNA Hybridization. *Chem. Commun.* **2008**, *48*, 6600–6602.
28. Niemeyer, C. M.; Bürger, W.; Hoedemakers, R. M. J. Hybridization Characteristics of Biomolecular Adaptors, Covalent DNA-Streptavidin Conjugates. *Bioconjugate Chem.* **1998**, *9*, 168–175.
29. Nangreave, J.; Yan, H.; Liu, Y. Studies of Thermal Stability of Multivalent DNA Hybridization in a Nanostructured System. *Biophys. J.* **2009**, *97*, 563–571.
30. Nangreave, J.; Yan, H.; Liu, Y. DNA Nanostructures as Models for Evaluating the Role of Enthalpy and Entropy in Polyvalent Binding. *J. Am. Chem. Soc.* **2011**, *133*, 4490–4497.
31. Ke, Y.; Liu, Y.; Zhang, J.; Yan, H. A Study of DNA Tube Formation Mechanisms Using 4-, 8-, and 12-helix DNA Nanostructures. *J. Am. Chem. Soc.* **2006**, *128*, 4414–4421.
32. Delgadillo, R. F.; Parkhurst, L. J. Spectroscopic Properties of Fluorescein and Rhodamine Dyes Attached to DNA. *Photochem. Photobiol.* **2010**, *86*, 261–272.
33. Murakami, A.; Nakaura, M.; Nakatsuji, Y.; Nagahara, S.; Tran-Cong, Q.; Makino, K. Fluorescent-Labeled Oligonucleotide Probes: Detection of Hybrid Formation in Solution by Fluorescence Polarization Spectroscopy. *Nucleic Acids Res.* **1991**, *19*, 4097–4102.
34. Kumke, M. U.; Li, G.; Linn, C. P. Hybridization of Fluorescein-labeled DNA Oligomers Detected by Fluorescence Anisotropy with Protein Binding Enhancement. *Anal. Chem.* **1995**, *67*, 3945–3951.
35. Torimura, M.; Kurata, S.; Yamada, K.; Yokomaku, T.; Kamagata, Y.; Kanagawa, T.; Kurane, R. Fluorescence-quenching Phenomenon by Photoinduced Electron Transfer between a Fluorescent Dye and a Nucleotide Base. *Anal. Sci.* **2001**, *17*, 155–160.
36. Crockett, A. O.; Wittwer, C. T. Fluorescein-labeled Oligonucleotides for Real-Time PCR: Using the Inherent Quenching of Deoxyguanosine Nucleotides. *Anal. Biochem.* **2001**, *290*, 89–97.
37. Doose, S.; Neuweiler, H.; Sauer, M. Fluorescence Quenching by Photoinduced Electron Transfer: Reported for Conformational Dynamics of Macromolecules. *ChemPhysChem.* **2009**, *10*, 1389–1398.
38. Craig, M. E.; Crothers, D. M.; Doty, P. J. Relaxation Kinetics of Dimer Formation by Self Complementarity Oligonucleotides. *Mol. Biol.* **1971**, *62*, 383–392.
39. Ke, Y.; Nangreave, J.; Yan, H.; Lindsay, S; Liu, Y. Developing DNA Tiles for Oligonucleotide Hybridization Assay with Higher Accuracy and Efficiency. *Chem. Commun.* **2008**, *43*, 5622–5624.
40. Zhang, Z.; Zeng, D.; Ma, H.; Feng, G.; Hu, J.; He, L.; Li, C.; Fan, C. A DNA-Origami Chip Platform for Label-Free SNP Genotyping Using Toehold-Mediated Strand Displacement. *Small* **2010**, *6*, 1854–1858.
41. Yurke, B.; Mills, A. P. Using DNA to Power Nanostructures. *Genet. Program. Evol. Mach.* **2003**, *4*, 111–122.
42. Zhang, D. Y.; Winfree, E. Control of DNA Strand Displacement Kinetics Using Toehold Exchange. *J. Am. Chem. Soc.* **2009**, *131*, 17303–17314.